Iraqi National Journal of Earth Science, Vol. 26, No. 3, 2026(89-98)

Iraqi National Journal of Earth Science

www.earth.uomosul.edu.iq

Detecting Seepage Paths and Karst Phenomenon in the Upstream of Beduh Dam, Northern Iraq via Electrical Resistivity Tomography

Jalal H. Younis [1*], **Alfred A. Mansour** [2], **Chiman I. Ahmed** [3]

jalal.younis@uod.ac alfredgeo77@gmail.com chiman.ahmad@uod.ac

[1] *Department of Geology, College of Science, University of Duhok, Duhok, Iraq.*
[2] *Directorate of Groundwater-Branch Duhok, Ministry of Agriculture, Kurdistan Region of Iraq.*
[3] *Department of Geology, College of Science, University of Duhok, Duhok, Iraq.*

Received: 16 March 2025 Received in revised form: 18 April 2025 Accepted: 18 May 2025
Available online: 01 July 2026

Abstract

An Electrical Resistivity Tomography (ERT) investigation was conducted at the Beduh earth dam in northern Iraq (Kurdistan Region) to identify leakage channels within the subsurface structure next to the dam body. The survey was conducted along four linear measurement traverses: traverses 1, 2, and 4 measured 300 meters each, while traverse 3 measured 200 m. All traverses were taken in the upstream part of the dam. Two traverses were located on the sides of the dam's embankment, one was in the middle, and the fourth (Traverse 3) was perpendicular to them, running in a north-south direction parallel to the dam body. The examination of the inverted ERT sections indicated the presence of cracks, seepage paths, and karst phenomena within the limestone formations that comprise the top surface of the bedrock in the dam reservoir. Numerous subsurface structural abnormalities were identified within the fractured bedrock, predominantly linked to potential karstic cavities, voids, and discontinuities in the carbonate rocks. Furthermore, the results indicated the presence of a notable subsiding structure aligned with the main valley trajectory. It is posited that the highly fractured bedrock and other identified characteristics may be the main sources of water leakage from the dam's reservoir.

Keywords:

Seepage, karst, Beduh dam, Electrical Resistivity Tomography (ERT)

DOI: 10.33899/injes.v26i3.60925, *©Authors, 2026, College of Science, University of Mosul.*
This is an open-access article under the CC BY 4.0 license (http://creativecommons.org/licenses/by/4.0/).

==========

1. Introduction

The electrical resistivity tomography (ERT) approach is one of the most effective geophysical techniques for many shallow subsurface investigations, such as engineering investigations (Ahmed et al., 2025; Al-Mashhadany et al, 2024) and mapping the saturation degree of water and other liquids in the vadose zones (Cardarelli et.al., 2014; Sanuade and Ismail, 2023). This method is one of the non-invasive sensing technologies. Electrical resistivity tomography is a commonly employed technique for detecting seepage. It relies on the physical characteristics of resistivity and can be integrated with other geophysical methods to minimize the multi-solution issues and enhance detection accuracy. The acquired images, appearing as resistivity pseudo-sections, are processed by inversion software to provide interpreted resistivity and depth values for the identified anomalies along the profile.

The strategic importance of dams in hydroelectric power generation, flood control, and water resource management underscores the imperative of ensuring their structural integrity (Ahn et al., 2014; Chaudhari and Pokhrel, 2022). Geophysical methods have proven essential for evaluating dam stability and mitigating environmental and socio-economic risks (Sanuade and Ismail, 2023).

The increasing utilization of geophysical techniques, such as electrical resistivity, seismic analysis, and ground-penetrating radar, in engineering and environmental projects can be attributed to their efficiency, cost-effectiveness, and comprehensive spatial coverage (Khatri et al.,

2011; Godio et al., 2006). These non-invasive methods provide valuable insights into subsurface conditions, facilitating informed decision-making (Chaudhari and Pokhrel, 2022).

The application of Electrical Resistivity Tomography (ERT) has substantially advanced subsurface investigations, yielding critical information on geological and hydrological processes (Ahmed et al., 2025; Al-Mashhadany et al, 2024). Specifically, ERT's detection of seepage pathways informs groundwater flow modeling and environmental impact assessments (Loke and Barker, 1996).

Beyond seepage detection, ERT effectively identifies subsurface karst structures, including sinkholes, cavities, and channels.

The application of Electrical Resistivity Tomography (ERT) is integral to groundwater protection and management, particularly in karst environments where geological features significantly influence water quality and availability. Detailed resistivity data analysis facilitates the mapping of karst structures, providing critical insights that support environmentally sound decision-making processes (Keller and Frischknecht, 1996).

Furthermore, Electrical Resistivity Tomography (ERT) plays a pivotal role in characterizing subsurface groundwater resources, providing a non-invasive approach to assess aquifer properties and distribution. By enabling precise mapping of groundwater reservoirs and estimating potential yields, ERT informs sustainable water management strategies, particularly in arid and semi-arid regions (Zhou, 2019).

Sufiyanussuari et al. (2021) highlight ERT's efficacy in detecting saturated materials (resistivity <100 ohm.m), guiding targeted groundwater exploration. Identifying GPZs is vital for ensuring long-term groundwater sustainability, minimizing depletion risks, and maintaining equitable distribution.

The identification of groundwater potential zones through Electrical Resistivity Tomography (ERT) improves our understanding of aquifer recharge areas and their connectivity, thereby facilitating more effective water resource management and conservation strategies (Atekwana and Slater, 2009). Together, these applications highlight the importance of ERT in enhancing our comprehension of subsurface hydrology and geology.

The objective of this work is to assess the geo-structural conditions of the hidden bedrock and determine the seepage route along the upstream section of the dam site, as well as to identify any cracks, faults, and caves in the vicinity, particularly beneath the reservoir bed.

2. Location of the study area

Beduh Dam is located 6km to the northeast of Kani Mase District. The name of the dam comes from the nearby village that holds the same name. Figure 1 shows the location of the dam on the Iraqi administrative map.

Fig. 1: The location of Beduh Dam

Table 1 shows the elevation, trend, and the locations of both ends of each ERT traverse used in this study.

Table 1: The elevation, trend, and the locations of both ends of each ERT traverse

	Start and end of electrodes	UTM (E)	UTM(N)	Elevation(m) a.s.l.
Geophysical Traverse_1	Electrode no.1	357283	4125335	1415
	Electrode no.60	356993	4125354	1417
Geophysical Traverse_2	Electrode no.1	357360	4125282	1426
	Electrode no.60	357069	4125300	1435
Geophysical Traverse_3	Electrode no.1	357239	4125410	1428
	Electrode no.48	357236	4125220	1446
Geophysical Traverse_4	Electrode no.1	357348	4125401	1427
	Electrode no.60	357057	4125389	1426

3. Geology of the study area

Depending on the structural geology of Iraq, the study area is located within the thrust zone, the South limb of the Ora Anticline (Fig. 2). The rock units' outcrops (Fig. 3) show that the dam site is

covered mainly by Beduh, Mirga Mir, and Chia Zairi geological Formations at the center of the dam and both embankments as well, from Lower Triassic to Upper Permian age (Fig. 4).

The geology of the dam site includes thick bedded limestone from the Upper Permian at the left abutment, clay-clayey limestone-shale alternations from the Lower-Middle Triassic, actual slope deposits at the right abutment, and alluvium at the base of the stream (Figure 3). The lower limestone exhibits a well-bedded and partially dolomitic nature, displaying karstic dissolution characteristics. The geology on the right side comprises Lower-Middle Triassic-aged shale, calcareous clay, and clayey limestone alternations, which appear brownish to greenish in color in the field.

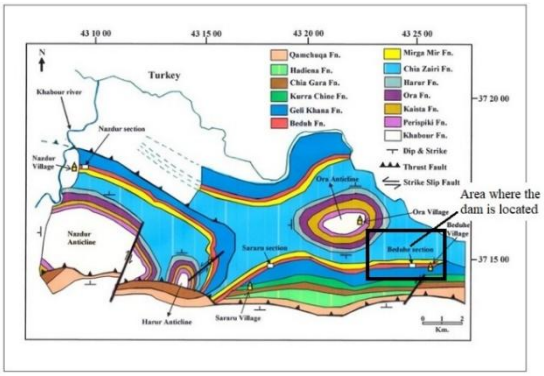

Fig. 2: Geological map of the area and the studied sections (after Al-Brifkani, 2008)

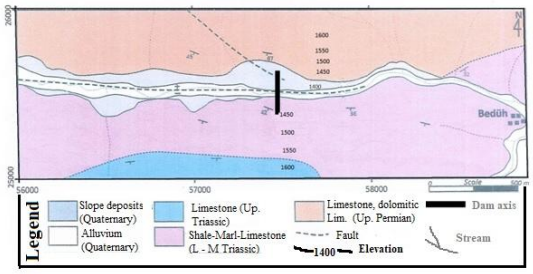

Fig. 3: An enlarged geological map of the Beduh dam site

The Beduh Shale Formation (Triassic); Lithology: Red-brown and purplish shales and marls, some silty, with subordinate thin ribs of limestone with sandy streaks.

Mirga Mir Formation (Lower Triassic); Lithology: Thin-bedded, grey and yellow, marly limestones and shales with slump beds and recrystallization breccias; oolitic limestones at base, with wisps of sandstone.

Chia Zairi Limestone Formation (Upper Permian); Lithology: Upper unit thin-bedded, dark blue limestones, with groups of harder, more massive, silicified, scarp-forming limestones. Middle unit vacuolar dolomites with solution and recrystallization breccia. Lower unit: alternating thin-bedded, dark blue, organic-detrital limestone.

Mirga Mir, underlying formation and details of contact: Chia Zairi limestone formation; contact conformable and gradational over a narrow interval, taken at the base of a thick succession of thin-bedded, soft limestones and silty marls, and above massive dolomitic limestones of the Permian. Overlying formation and details of contact. Beduh Shale Formation; contact gradational, conformable, taken at the color change from grey and yellow below to red and purple above. The recent sediments are composed of slope deposits and alluvium (Figure 3).

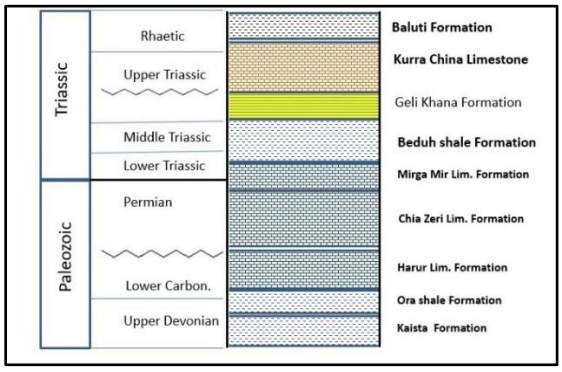

Fig.4: Stratigraphic column of the geological units' outcrops in the study area.

Slope deposits include boulder-sized limestone fragments in a brownish clay-mud matrix. The geometry and morphology of the slope materials (Figure 3) indicate sliding of this material towards the river base.

Actual river deposits-alluvium occur along the river, which shows a 40-70 m width. The main elements of the alluvium are composed of rounded and different-sized limestone, clayey limestone, and quartzite.

4. Methodology

The electrical resistivity method is a non-intrusive geophysical approach in which profiles were scattered along the upstream side of Beduh Dam, parallel to and near the dam embankment. Resistivity profiles have been used successfully to identify seepage routes in karsts/cavities under the dam's reservoir bed. Geophysical resistivity techniques are based mostly on materials' intrinsic electrical resistance and resistance contrasts. The resistivity of earth materials is calculated by introducing an electrical current into the ground and measuring the resultant potential difference.

4.1. Fieldwork

Resistivity 2D was used in the field by using Syscal Switch RI 72 (Fig. 5). Four traverses were conducted in the Upstream Dam location, using the Wenner-Schlumberger configuration for electrodes with a space of 5 m and a length equal to 295 m, three of them were parallel to each other and perpendicular to the dam axis, one in the center and the other two at both stream banks. The fourth traverse has an electrode space of 4 m and a length equal to 192 m, which runs parallel to the Dam axis (Fig. 6). The coordinates of the intersection points between traverse 3, which crosses all other traverse lines, are shown in Table 2

The collected field data is saved in a text file within the resistivity meter memory. The data obtained from the field is transferred through a serial link from the memory of the resistivity meter to the computer before converting the field data to a suitable format and exporting it to RES2DINV software version 3.58 for interpretation. To obtain a model that is closest to the real geology, the inversion of the sounding is carried out by Res2DINV, which is a computer program that will automatically determine a two-dimensional resistivity model of the subsurface for the data obtained from electrical imaging surveys. The quality of the recorded data is good, as it appears from the similarity between the measured and the calculated apparent resistivity section.

The preprocessing of the received data was necessary to carry out to find the outliers caused by the lateral variation of the geologic units and the low electrode conduct.

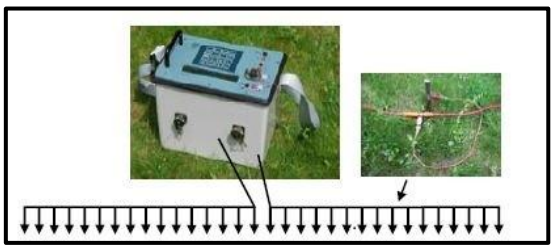

Fig. 5: Syscal Switch Multi-Electrode Equipment.

Table 2: The coordinates of the intersection points between traverse-3 (North-South) and all other traverses (East-West).

Intersection of:	Longitude (UTM)	Latitude (UTM)
Traverse 3 with traverse 1	357239 E	4125338 N
Traverse 3 with traverse 2	357237 E	4125292 N
Traverse 3 with traverse 4	357241 E	4125401 N

4.1.1. Traverse-1:

The extension of the traverse is east-west, as shown in Fig. 6, located in the stream center approximately parallel to the beds' strike direction in the area, and its length is 295 m with electrodes spaces 5 m. As shown in the cross-section below, Fig 7, three main resistivity zones have been identified. The first one on the top has a thickness of about 7 m with a high resistivity value (100–250) ohm.m distributed along the section, representing boulders, pebbles, and gravel of river Terraces; the second zone has a resistivity value of 13-100 ohm.m. The cross section shows that faults have affected the bedrock, and some fissures and caves are expected (blue color). A seepage path appears at stations between (25-35) m, and a thickness of (20) m represents the Mirga Mir Formation, which consists of marly limestone, marl, and shale with a highly fractured and saturated zone (expected cave or karst) under stations between (75-130) m and under stations between 235-260 m. The Last zone, which appears at a depth of 25 m, represents the Chia Zairi Formation and has a high resistivity value between 110-280 ohm.m of fractured limestone and Dolomitic limestone, with a thickness of about 12-15 m.

4.1.2. Traverse-2:

Located at the right embankment of the dam, parallel to the bed strike direction and to Traverse_1, the extension of this traverse is east-west (Fig. 6), and its length is 295 m with electrode spacing of 5 m. As appears in the cross section below (Fig 8), three main resistivity zones have been detected as well; the first one on the top of the right part has a thickness of about 5- 10 m with a low resistivity value of 25-65 ohm.m, representing shale of the Beduh Formation.

The second zone has a resistivity value between 70-160 ohm.m, with different thickness due to fault movement. On the right side (west), the thickness is about 10 meters, while on the left side (east), it is about 30 meters. The latter represents the Mirga Mir Formation, which consists of marly limestone, shale, and marl. This zone has high fracture density and has been affected by local faults.

The last zone appears only on the right side at a depth of 27 m and has a high resistivity value (200-650) ohm.m, representing the Chia Zairi Formation, which consists of limestone (fractured)

and dolomitic limestone. Fault detected between stations (130-150) m; also, a saturated and fractured zone was detected between stations (80-90) m at a depth of 35 m.

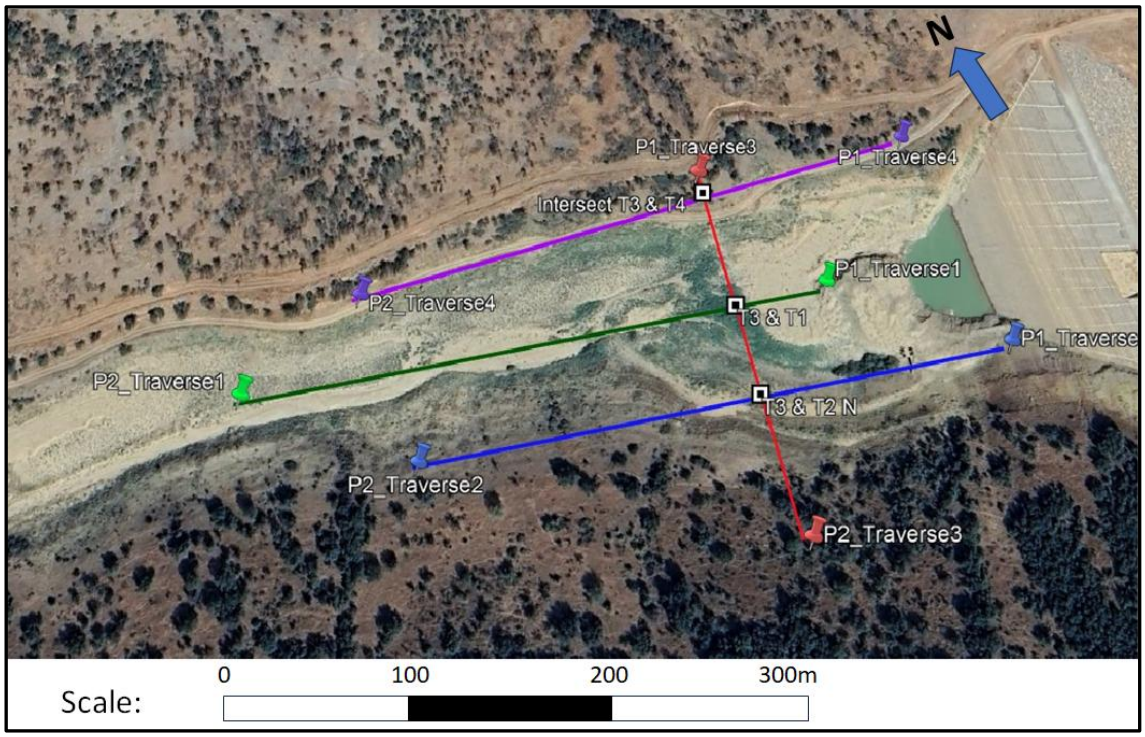

Fig. 6: Google map shows the location of the 2D geophysical traverses.

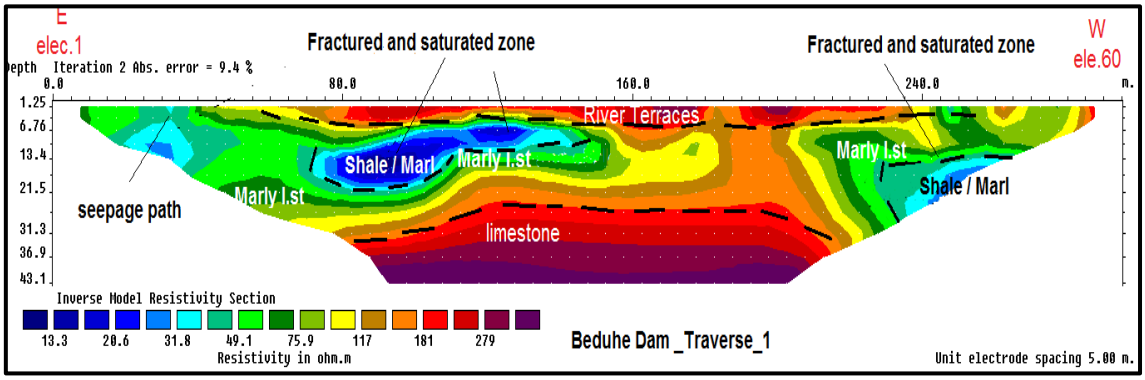

Fig. 7: The interpretation of 2D resistivity Traverse-1.

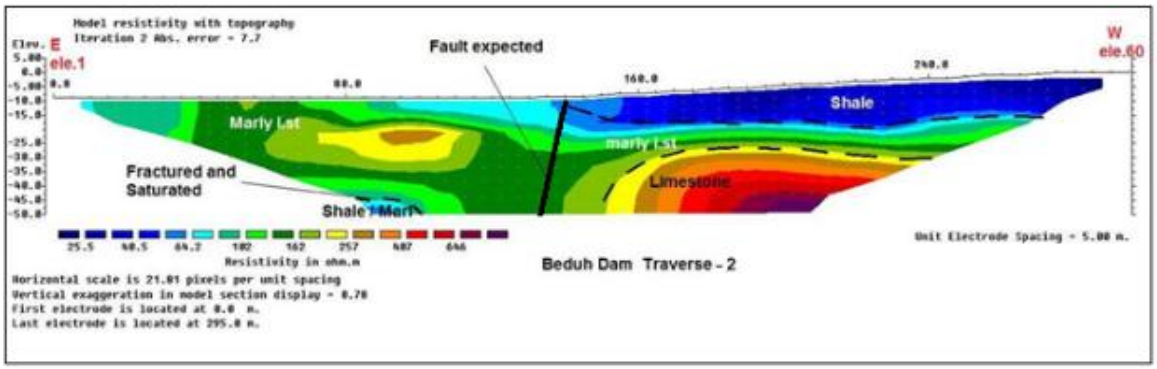

Fig. 8: The interpretation of 2D resistivity traverse-2.

4.1.3. Traverse-3

The extension of this traverse is North-South (fig. 6), approximately perpendicular to the beds' strike direction in the area, and parallel to the Dam axis. Its length is 192 m with an electrode spacing of 4 m. As appears in the cross-section below (Fig. 9), the dips of strata are clear and tilted to the south direction.

River Terraces are distributed from the middle of the upper part toward the left side, from station 44 to station 72 m. two main resistivity zones were determined, first one on the top has low resistivity value (25–100) ohm.m distributes along the section represented thickness about 20 m from the middle to the North side and has thickness about 30 m from middle to the south side of cross section, represented the Mirga Mir Formation consists of shale, marl, and marly limestone, highly fractured and saturated zone, cave detected between stations (48-680m. The second zone has a high resistivity value (100-250) ohm.m and a thickness of about 15 m in the lower middle part and decreases to 5 m thick towards the north side, representing the Chia Zairi Formation, which consists of limestone and dolomitic limestone (fractured and saturated).

Fault expected between the Mirga Mir Formation and Chia Zairi Formation (centre of the profile). Seepage path identified between stations (76-104) m.

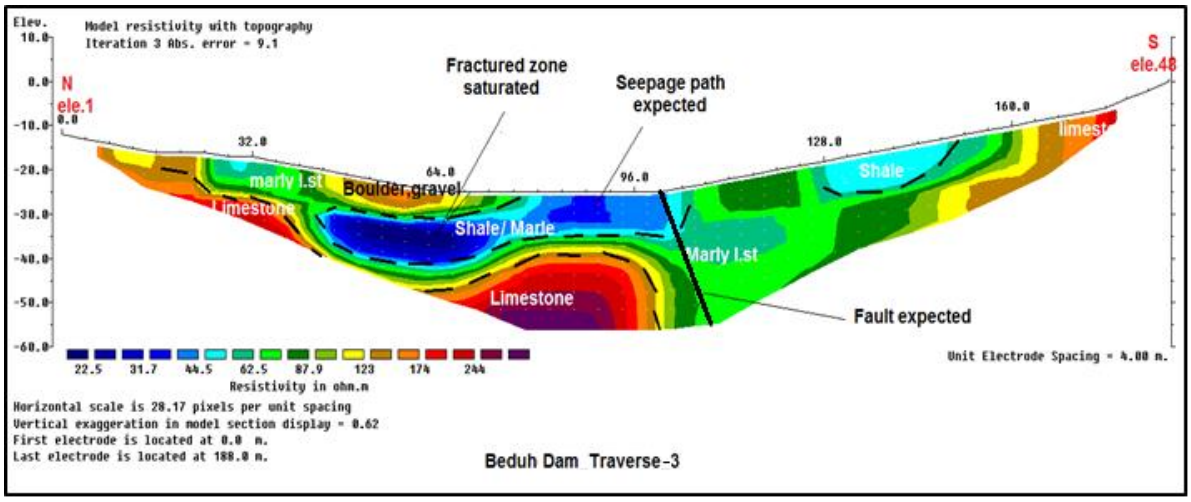

Fig. 9: The interpretation of 2D Resistivity Traverse-3.

4.1.3. Traverse-4

The extension of the traverse is East- West (Fig. 6); it is parallel to the bed strike and to Traverse_1 and Traverse_2. Its length is (295) m with electrode spacing (5) m. As appears in the cross-section below (Fig 10), two main resistivity zones are identified. The first one on top of the cross-section has a thickness of about (15-20) m with a resistivity value of (50–160) ohm.m distributed along the section, representing slope deposits of limestone, marly limestone, and shale. The second zone consists of limestone and dolomitic limestone (fractured) that belong to the Chia Zairi Formation, appearing at a depth of 15 m; it has a high resistivity value of 200-500 and a thickness of about 25 m. Disappearing this zone on the East side of the cross section between stations (55-90) m indicates the presence of a fault that strikes the area, which is caused by highly fissured zones, fractures, and a saturated zone identified as a cave or void was detected in the cross section (Fig. 10).

When we placed and dropped the interpreted geophysical resistivity profiles directly onto their location on the Google Earth map figures (11) and (12), it turned out that the locations of the faults in the geophysical sections completely matched the lineament faults visible on the Earth's surface, which confirms the validity of the interpretation results.

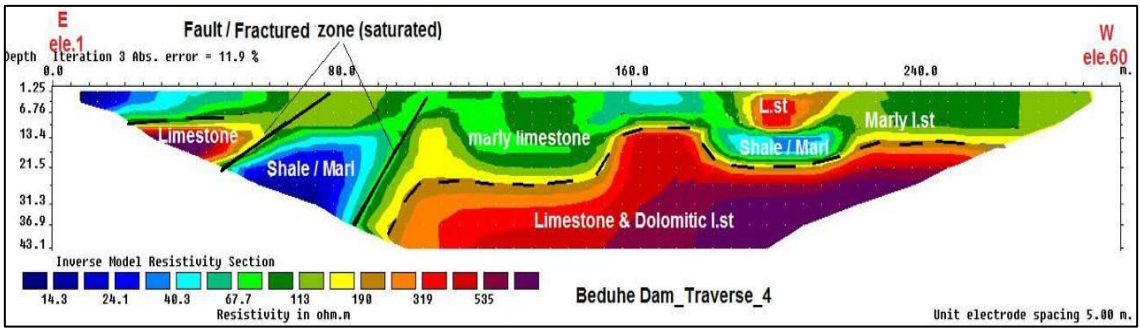

Fig. 10: The interpretation of 2D Resistivity Traverse-4 with topography

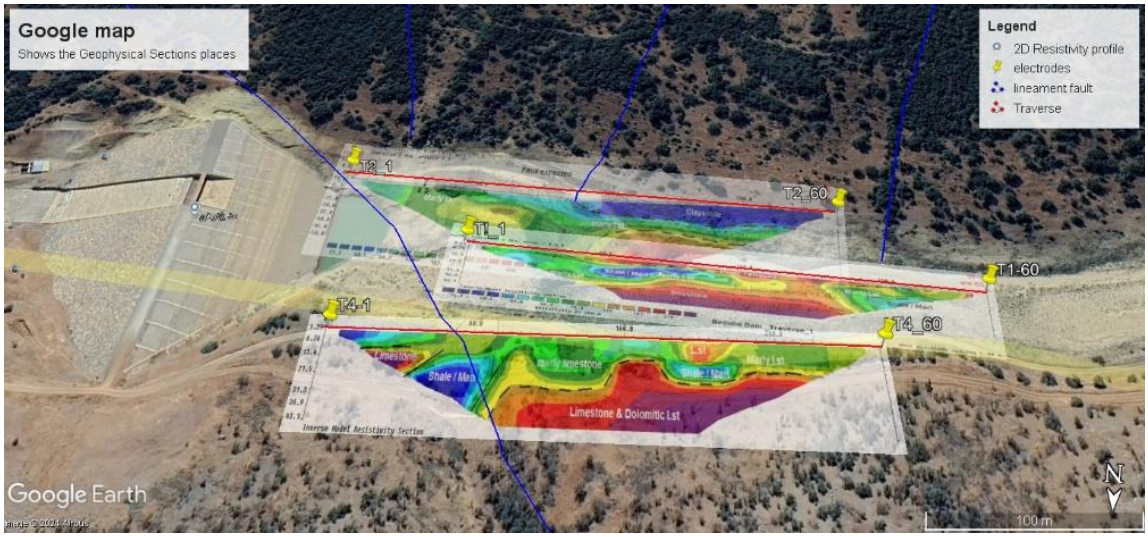

Fig. 11: Shows the location of the 2D Resistivity profiles (Traverses-1, 2, and 4) on the Google map

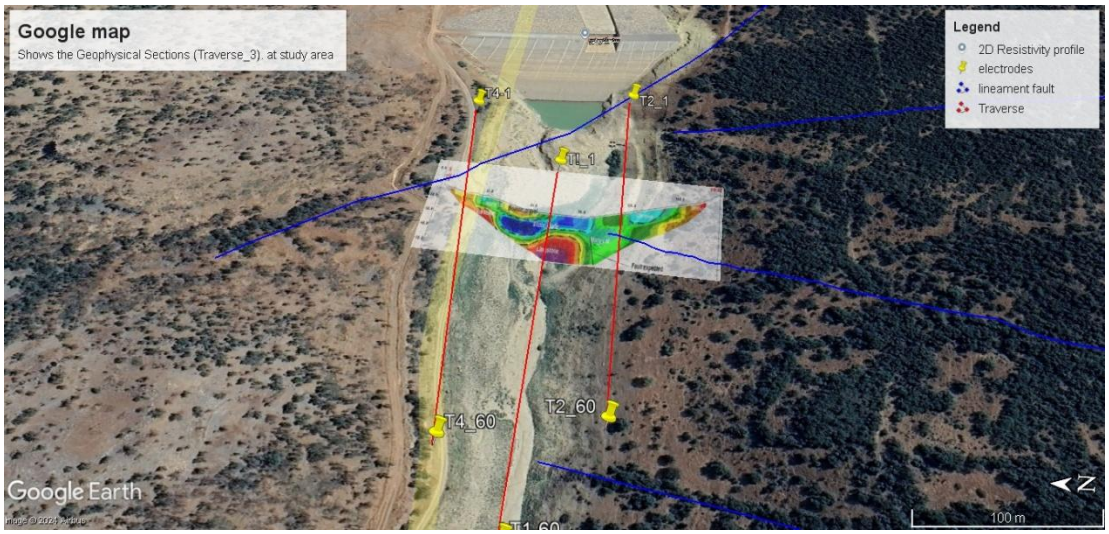

Fig. 12: Shows the location of the 2D Resistivity profile (Traverse-3) on the Google map.

5. Conclusions and Recommendations:

The interpretation results of all geophysical traverses show and provide the following outcomes:

The presence of weak areas, such as joints, fractures, and caves, that might be a result of being affected by faults and thrust zones. The trend of the main fault plane, the strike of the fault, is east-west in the middle of the channel basin, which was identified in the third Traverse (Traverse-3), located between the Chia Zairi Formation and Mirga Mir Formation. At least two more faults were detected perpendicular to the stream and

parallel to the dam axis; it seems to have continuity on both sides, as shown in traverses (1, 2, and 4). Additionally, a fault that runs parallel to the bedding plane, called a listric fault, has also been identified besides the faults that intersect the bedding plane.

Water seepage into subsurface layers was identified in Traverse-1 and Traverse-3 in the middle of the stream, which is located approximately 100 m away from the upstream toe of the dam. There is a high probability of cavities, likely karsts, and fractures and joints below this area. This zone is linked with the same fractured zone located in traverses 2 and 4. This part represents the fault plane where the vicinity is highly fractured, pervious, and saturated with water. Another fracture zone and cave were identified and located about 320 m from the dam body in the middle part of the stream, as shown in Traverse-1. It follows the same trend as the suspected fault lineament identified in the area.

The water seepage mostly follows a trajectory from the center towards the right abutments along the fault line, which is marked by many joints and fractures. Additionally, it extends in a south-eastern direction through the fractured marly limestone strata of the Mirga Mir Formation. This seepage occurs along the bedding plane of the strata, which serves as conduits for water transmission. The lateral variation of the strata and formations parallel to the dam axis represents a vulnerability and potential for water leakage at the contact zones, i.e., the bedding planes between geological units or formations.

The aforementioned results indicate that the dam is solely applicable for flood protection, as the upstream region of the dam reservoir is situated in a highly fractured zone, thereby augmenting the seepage and infiltration of surface water into the ground.

One of the advantages of this dam is also to have a large-scale recharge area for groundwater.

This study concludes that grouting of the joints and fractures is inadvisable due to the excessively high frequency of these joints.

A recommendation is to cover the channel bed with a blanket of a one-meter-thick layer of compacted soil to reduce seepage and infiltration while simultaneously enhancing the dead storage capacity of the dam reservoir.

It is highly recommended to carry out at least one supplementary traverse that intersects perpendicularly with traverse number two. This will more distinctly illustrate the extent and width of the karst situated in the eastern region, namely, adjacent to the dam structure.

6. References

Ahmed, M.S., Al-Juraisy, B.A., Al-Mashhadany, A.Y., 2025. Using Azimuthal Resistivity Survey Technique to determine Subsurface Fractures of Quaternary Deposits in the University of Mosul - Northern Iraq. Iraqi National Journal of Earth Science, 25 (1), 34-49, DOI: https://10.33899/earth. 2024.146105.1219.

Ahn, J.M., Lee, S., Kang, T., 2014. Evaluation of dams and weirs operating for water resource management of the Geum River. Sci. Total Environ., 478, pp. 103–115. https://doi.org/10.1016/j.scitotenv.2014.01.038 .

Al-Brifkani, M.J.N. (2008). Structural and Tectonic Analysis of the Northern Thrust Zone (East Khabour River) in Iraq. Unpublished Ph.D. Thesis, University of Mosul, 174 P. (In Arabic).

Al-Mashhadany, A.Y., Al-Juraisy, B.A., Ahmed, M.S., 2024. Detecting the effect of soil compaction processes on the distribution of subsurface resistivity using 2D resistivity imaging. Iraqi National Journal of Earth Science, 24 (2), 62-71. DOI:https://doi.org/10.33899/earth.2023.142652.1131

Boulange, J., Hanasaki, N., Yamazaki, D. et al., 2021. Role of dams in reducing global flood exposure under climate change. Nat Commun., 12, 417. https://doi.org/10.1038/s41467-020-20704-0 .

Cardarelli, E.; Cercato, M.; De Donno, G., 2014. Characterization of an earth-filled dam through the combined use of electrical resistivity tomography, P-and SH-wave seismic tomography and surface wave data. J. Appl. Geophys., 106, pp. 87–95. https://doi.org/10.1016/j.jappgeo.2014.04.007

Chaudhari, S. and Pokhrel, Y., 2022. Alteration of river flow and flood dynamics by existing and planned hydropower dams in the Amazon River Basin. Water Resour. Res., 58, e2021WR030555. https://doi.org/10.1029/2021WR030555

Cooper, A.H. and Waltham, A.C., 1999. Subsidence caused by gypsum dissolution at Ripon, North Yorkshire. Q. J. Eng. Geol., 32, pp. 305–310. https://doi.org/10.1144/GSL.QJEG.1999.032.P4.01.

Cosenza, P., Marmet, E., Rejiba, F., Jun Cui Y., Tabbagh, V. and Charlery, Y., 2006. Correlations between geotechnical and electrical data: A case study at Garchy in France, Journal of Applied Geophysics, 60, pp. 165-178. https://doi.org/10.1016/j.jappgeo.2006.02.003

Godio, A., Strobbia, C. and De Bacco, G., 2006. Geophysical characterisation of a rockslide in an alpine region, Engineering Geology, 83, pp. 273-286. https://doi.org/10.1016/j.enggeo.2005.06.034

Gołębiewski, T., Piwakowski, B., Cwiklik, M., and Bojarski, A., 2021. Application of combined geophysical methods for the examination of a water dam subsoil. Water, 13, 2982. https://doi.org/10.3390/w13212981

Guerrero, J., Gutiérrez, F., and Lucha, P., 2004. Paleosubsidence and active subsidence due to evaporite dissolution in the Zaragoza city area (Huerva River valley, NE Spain). Processes, spatial distribution and protection measures for linear infrastructures. Eng. Geol., 72, pp. 309–29. https://doi.org/10.1016/j.enggeo.2003.10.002

Gutierrez, F. and Cooper, A.H., 2002. Evaporite dissolution subsidence in the historical city of Calatayud, Spain: damage appraisal and prevention. Nat. Hazards, 25, pp. 259–88. https://doi.org/10.1023/A:1014807901461

Hyatt, J.A. and Jacobs, P.M., 1996. Distribution and morphology of sinkholes triggered by flooding following tropical storm Alberto at Albany, Georgia, USA. Geomorphology, 17, pp. 305–316. https://doi.org/10.1016/0169-555X(96)00014-1

Johnson, K.S., 2008. Gypsum-karst problems in constructing dams in the United States. Environ. Geol., 53, pp. 945–955. https://doi.org/10.1007/s00254-007-0720-z

Keller, G.V., and Frischknecht, F.C., 1996. Electrical Methods in Geophysical Prospecting. Pergamon Press.

Khatri, R., Shrivastava, V.K. and Chandak, R., 2011. Correlation between vertical electric sounding and conventional methods of geotechnical site investigation. International Journal of Advanced Engineering Sciences and Technologies, 4, pp. 042-053.

Loke, M.H., and Barker, R.D., 1996. Rapid least-squares inversion of apparent resistivity pseudosections by a quasi-Newton method. Geophysical Prospecting, 44(1), pp. 131-152. https://doi.org/10.1111/j.1365-478.1996.tb00142.x

Sanuade, O.; Ismail, A., 2023. Geophysical and geochemical pilot study to characterize the dam foundation rock and source of seepage in part of Pensacola Dam in Oklahoma. Water 2023, 15, 4036. https://doi.org/10.3390/w15234036

Sufiyanussuari, S.A., Tajudin S.A.A, Azmi, M.I.S, Zahari, M.N.H, and Muztaza, N.M., 2021. Groundwater Pathway Mapping Using Electrical Resistivity Tomography (ERT) Method. Journal of Sustainable Underground Exploration, 1 (1), 32-37. http://publisher.uthm.edu.my/ojs/index.php/j-sue

Zhou, B., 2019. Electrical Resistivity Tomography: A subsurface-Image Technique. In "Applied Geophysics with Case Studies on Environmental, Exploration and Engineering Geophysics, Edited by Kanh, A.I. Intech Open. ISBN: 798-1-83880-740-5

Iraqi National Journal of Earth Science, Vol. 26, No. 3, 2026(89-98)

Iraqi National Journal of Earth Science

www.earth.uomosul.edu.iq

الكشف عن مسارات التسرب والظاهرة الكارستية في أعالي حوض سد بيدوه – شمال العراق عبر التصوير المقطعي بالمقاومة الكهربائية

جلال حسن يونس[1]* ، **ألفريد عبد الأحد منصور[2]** ، **جيمن إسماعيل أحمد [3]**

jalal.younis@uod.ac alfredgeo77@gmail.com chiman.ahmad@uod.ac

[1] *قسم علوم الأرض، كلية العلوم، جامعة دهوك، دهوك، العراق.*

[2] *مديرية المياه الجوفية – فرع دهوك، وزارة الزراعة، إقليم كردستان العراق.*

[3] *قسم علوم الأرض، كلية العلوم، جامعة دهوك، دهوك، العراق.*

تاريخ الاستلام: 16 اذار 2025 تاريخ المراجعة: 18 نيسان 2025 تاريخ القبول: 18 ايار 2025

تاريخ النشر الالكتروني: 01 تموز 2026

الملخص

تم إجراء مسح مقطعي للمقاومة الكهربائية في سد بيدوه الترابي في شمالي العراق (إقليم كردستان) لتحديد قنوات التسرب عبر الصخور تحت السطحية المجاورة لجسم السد. تم إجراء المسح على طول أربعة مسارات قياس خطية، يبلغ قياسها 300 متر للمقطعين 1 و2 و4 بينما يبلغ 200 متر للمقطع 3. تم أخذ جميع هذه المقاطع العرضية في الجزء العلوي من السد. اثنان على جانبي حوض السد، وواحد في منتصف الطريق، في حين أن المقطع الرابع(الذي يحمل المقطع رقم 3) كان عمودي عليهما ويذهب في الاتجاه الشمالي الجنوبي الموازي لجسم السد. اشارت نتائج تفسير المقاطع الى تواجد الشقوق ومسارات التسرب وظاهرة الكارست في تكوينات الحجر الجيري التي تشكل السطح العلوي من صخور الأساس لخزان السد. تم الكشف عن العديد من التشوهات البنيوية تحت السطحية داخل طبقة الأساس المتصدعة، والتي ترتبط بشكل أساسي بالتجاويف الكارستية المحتملة والفراغات والانقطاعات المتكونة في الصخور الجيرية. وعلاوة على ذلك، أشارت النتائج إلى تواجد بنية هبوط ملحوظة تتماشى مع مسار الوادي الأساسي. ومن المفترض أن طبقة الأساس المتصدعة للغاية والخصائص الأخرى المحددة هي المصادر الأساسية المحتملة لتسرب المياه من خزان السد.

الكلمات المفتاحية:

التسرب، الكارست، سد بيدوه، التصوير المقطعي بالمقاومة الكهربائية(ERT).

DOI: 10.33899/injes.v26i3.60925, *©Authors, 2026, College of Science, University of Mosul.*

This is an open-access article under the CC BY 4.0 license (http://creativecommons.org/licenses/by/4.0/) .

==========